Geochemical Perspectives Letters

© 2021 The Authors
Published by the European Association of Geochemistry

Early differentiation of magmatic iron meteorite parent bodies from Mn–Cr chronometry

A. Anand, J. Pape, M. Wille, K. Mezger, B. Hofmann

Supplementary Information

The Supplementary Information includes:

1. Samples and Analytical Methods

Seven samples from IIAB, IIIAB and IVA iron meteorite groups were analysed in this study. Chromite from whole rock iron meteorites, Sikhote Alin, Agoudal & Cape York and daubréelite from samples NWA 11420, Yanhuitlan & Duchesne (all from the Natural History Museum Bern) were separated. Pre-isolated chromite grains from sample Saint Aubin were received from the Natural History Museum Vienna. Sample collection numbers are provided in Table 1. At the University of Bern, chromite grains were identified using an optical microscope and isolated in small whole-rock fragments. The fragments were hand crushed using a pre-cleaned agate mortar and treated in conc. aqua regia on a hot plate set to 90 °C for 48 h to completely dissolve the metal-sulphide dominated matrix, leaving behind residual chromite grains. To separate daubréelite, whole meteorite fragment or troilite (sulphide) nodules were treated with conc. aqua regia at room temperature for 12 h and the residue was further separated into a magnetic and non-magnetic fraction using a magnet. Daubréelite grains were isolated from the non-magnetic portion and confirmed with energy dispersive X-ray spectroscopy (EDS) on a ZEISS EVO50 SEM. Consecutively, individual grains were handpicked. Chromite and daubréelite grains weighing 1–3 mg from all the samples were transferred to a 7 mL Savillex® vial with 150–250 mg ammonium bifluoride (ABF, $NH_4F{\cdot}HF$, Sigma-Aldrich®, Trace Metal grade) and completely digested following the protocol described in O'Hara *et al.* (2017). The sample and reagent mixture was thermalized in a convection oven set to 230 °C for 48 h. Upon cooling, the mixture was dried down twice, first after treatment with 2 mL conc. HNO_3 and then after treatment with 1 mL conc. HNO_3 and 2 mL MilliQ® water.

Before chemical separation, an aliquot from digested chromite/daubréelite fraction from each sample was diluted in 10 mL 0.5 M HNO_3 to target for a 10 ppb Cr solution. These aliquots were used to determine Cr, Mn, and Fe concentrations using a 7700x Agilent ICP-MS at the Institute of Geography, University of Bern. Uncertainties on

Mn/Cr and Fe/Cr ratios are reported as 2 s.e. of the replicate measurements (n = 5) and remained <5 % for all the samples.

The procedure for Cr purification was adopted from Schoenberg *et al.* (2016). It includes three steps of a combination of cation–anion exchange chromatography modified after Schoenberg and von Blanckenburg, (2005) (column 1), Trinquier *et al.* (2008a) and Yamakawa *et al.* (2009) (column 2 and 3). In brief, an aliquot containing 15 µg Cr from each sample was taken up in 1 mL 6 M HCl and loaded on the first 7.5 mL Spectrum® polypropylene column containing 2 mL anion resin (BioRad® AG 1X8 100–200 mesh size). The Cr eluate from the first column was dried down, redissolved in 400 µL 6 M HCl, equilibrated on a hotplate set to 130 °C for ~30 min one day before the chemical separation and stored at room temperature overnight. The next day, the sample was re-equilibrated on a hot plate at 130 °C for one hour, diluted with 2 mL MilliQ® water to obtain 2.4 mL 1 M HCl and loaded on the second column filled with 2 mL cation resin (BioRad® AG 50W-X8 200–400 mesh size). The second column separation step produced a solution with mostly Cr, but incompletely separated from Ti and V. The third column with 0.5 mL BioRad® AG 50W-X8 200–400 mesh was used in order to obtain a clean Cr separate, free of Ti and V. The elute from the second column was dried down on a hot plate (at 90 °C), taken up in 0.5 mL conc. HNO_3 and dried down again immediately to transform the samples into nitrate form. The residue was redissolved in 3 mL 0.4 M HNO_3 for 30 min on a hotplate at 80 °C and let react cold for 5 days for the production of chloro-aquo complexes. Afterwards, each sample was loaded on the third column. The matrix was eluted in 8 mL 0.5 M HF and 9.5 mL 1 M HCl, and Cr was collected in 8 mL 4 M HCl. Finally, the Cr separate was redissolved in 100 µL conc. HNO_3 and dried immediately at 130 °C on a hotplate. This step was repeated two times until the residual organics from the column chemistry was completely destroyed. Typical recovery of Cr was in excess of 80 % for the whole column chemistry, determined by measurement of spiked sample solutions on an ICP-MS. Total chemistry blanks were below 10 ng, which are negligible compared to the µg range of Cr isolated and loaded on the filaments for each sample. The purified Cr was dissolved in a sufficient amount of 6 M HCl to yield a solution with a Cr concentration of *ca.* 1 µg/µL for loading on Re filaments for mass spectrometry. 1 µg/µL Cr was mixed with 1.4 µL 4 % silica gel on a piece of Parafilm® and loaded on the filament, minimizing the spread of the sample droplet. 0.7 µL Al (1000 ppm) and 0.7 µL H_3BO_3 (5000 ppm B) was then added to the top of this mixture. After drying the mixture at around 0.8 A, the filament was heated slowly to a dull red glow for less than one second.

The samples were analysed by Thermal Ionization Mass Spectrometer using a Thermo Scientific TRITON Plus instrument at the Institute of Geological Sciences, University of Bern. Aliquots of each sample were loaded on multiple filaments and measured at ^{52}Cr signal intensity between 8 and 12 V (10^{-11} Ω resistor). Intensities of ^{50}Cr, ^{51}V, ^{52}Cr, ^{53}Cr, ^{54}Cr, ^{55}Mn and ^{56}Fe were measured on the Faraday cups L3, L2, L1, C, H1, H2 and H3, respectively (Trinquier *et al.*, 2008a). Alignment of all Cr peaks (peak scan) was ensured before each measurement and peak centre was monitored on ^{53}Cr in the centre cup. Isobaric interference of ^{54}Fe on ^{54}Cr was corrected by monitoring ^{56}Fe. The isotopes ^{49}Ti and ^{51}V were measured to correct for isobaric interferences on ^{50}Cr. However, the ^{49}Ti and ^{51}V intensities remained indistinguishable from background intensities for all samples, verifying successful separation of V and Ti from Cr during column chromatography. A typical run for a single filament consisted of 24 blocks with 20 cycles each (integration time = 8.389 s), obtained in static acquisition mode. Gain calibration was done once, at the beginning of every measurement day. Amplifiers were rotated and the baseline was measured after every block (baseline = 30 cycles, each of 1.05 s). The Cr standard reference material NIST SRM 979, was used as a terrestrial reference material. The ^{53}Cr/^{52}Cr and ^{54}Cr/^{52}Cr ratios were normalized to ^{52}Cr/^{50}Cr = 19.28323 (Shields *et al.*, 1966) by applying the exponential mass fractionation law and are reported as ε^iCr, where $\varepsilon^i\text{Cr} = ([^i\text{Cr}/^{52}\text{Cr}]_{\text{sample}} / [^i\text{Cr}/^{52}\text{Cr}_{\text{NIST SRM 979}}] - 1) \times 10^4$ and i = 53 or 54.

2. Precision and Accuracy of Cr Isotope Data

The ε^iCr (i = 53 or 54) reported for any one sample represent the mean of the replicate measurements (n = 7–13, Tables 1, S-1). The replicate measurements for each sample are used to determine the external precision reported as 2 s.e. (Tables 1, S-1). The isotope compositions of each sample are reported relative to the mean value of the standard reference material (NIST SRM 979) measured along with the samples in each measurement session (single

turret). The external precision (2 s.d.) for the standard reference material (NIST SRM 979) in each measurement session was ~0.1 for ε^{53}Cr and ~0.2 for ε^{54}Cr.

To estimate the analytical accuracy of Cr isotopic data, we evaluated the consistency of results obtained on both terrestrial standards and meteorite samples and compared to the published results. The Cr isotope data (ε^{53}Cr = 0.072 ± 0.066, ε^{54}Cr = 0.881 ± 0.120) for Allende (CV) agrees with ε^{53}Cr = 0.11 ± 0.02 and ε^{54}Cr = 0.95 ± 0.06, reported in Zhu *et al.* (2021). Cr isotope data for terrestrial rock standard IAG OKUM is also in good agreement with the Cr isotope data for terrestrial samples compiled in Zhu *et al.* (2021). Whole rock samples for an ordinary chondrite (Dergaon, H5) and Acapulcoite (RF 529) measured along with the iron meteorite chromite/daubréelite fractions are in good agreement with the literature (Zhu *et al*., 2021). Additionally, ε^{54}Cr = −0.779 ± 0.061 and ε^{53}Cr = −0.268 ± 0.029 for Saint Aubin chromite reported in the present study is in perfect agreement with ε^{54}Cr = −0.81 ± 0.08 and ε^{53}Cr = −0.28 ± 0.06 reported in Trinquier *et al.* (2007, 2008b).

3. Correction for Spallogenic Cr

Spallation reactions induced by cosmic-ray exposure (CRE) can alter ^{53}Cr/^{52}Cr and ^{54}Cr/^{52}Cr ratios in solar system objects. This alteration depends on the following parameters: (1) duration and intensity of cosmic ray exposure, (2) Fe/Cr ratio, and (3) shielding condition for any given sample/component. A particular advantage of analysing chromite and daubréelite in iron meteorites is that due to low Fe/Cr ratios in these phases, spallogenic contributions of ^{53}Cr and ^{54}Cr produced by galactic cosmic radiation (GCR) from Fe are negligible and hence no correction for spallogenic Cr is required (Trinquier *et al*., 2008b; Liu *et al*., 2019). Less suitable for dating is the iron metal of iron meteorites, because of its very high Fe/Cr combined with the typically long irradiation time in space for iron meteorites, which leads to significant production of spallogenic ^{53}Cr and ^{54}Cr that is difficult to correct for and results in high uncertainties. For instance, a Fe/Cr ratio of 0.5 (Fig. S-1b), which is typical in chromite and daubréelite would result in ε^{53}Cr and ε^{54}Cr excesses of 0.002 and 0.005, respectively, even if the CRE age for the iron meteorite is as high as 800 Ma (ε^{53}Cr and ε^{54}Cr excesses determined using equation given in Table 2 in Trinquier *et al*., 2007, and a ^{53}Cr and ^{54}Cr production rate of 2.9 × 10^{11} atoms/Ma in Fe targets from Birck and Allégre, 1985). This spallogenic ε^{53}Cr and ε^{54}Cr contribution is well within the analytical uncertainties of the Cr isotopic measurements reported here.

Liu *et al.* (2019) measured Cr isotopic composition of 16 iron meteorites belonging to different chemical groups and showed that the CRE can cause coupled excesses in ε^{53}Cr and ε^{54}Cr with a linear correlation line of ε^{54}Cr = (3.90 ± 0.03) × ε^{53}Cr. This correlation is independent of the duration and intensity of cosmic ray exposure, Fe/Cr ratio and shielding condition for any given sample/component and hence provide an alternate way to test the need for spallogenic Cr correction. Figure S-1a shows an ε^{54}Cr *vs.* ε^{53}Cr plot for the chromite and daubréelite separates from the analysed iron meteorites. The ε^{54}Cr and ε^{53}Cr values show no correlation for the analysed chromite/daubréelite fractions and corroborates to the negligible spallogenic contribution in these components.

4. Summary of $(^{53}Mn/^{55}Mn)_i$ and $\varepsilon^{53}Cr_i$

Table S-3 provides a compilation of solar system initial $(^{53}Mn/^{55}Mn)_i$ and $\varepsilon^{53}Cr_i$ reported by different methods/approaches in the literature. Shukolyukov and Lugmair (2006), Moynier *et al.* (2007) and Göpel *et al.* (2015) determined the solar system initial $(^{53}Mn/^{55}Mn)_i$ and $\varepsilon^{53}Cr_i$ by evaluating the Mn/Cr data for bulk rock carbonaceous chondrites (CC) on a ^{55}Mn/^{52}Cr *vs.* ε^{53}Cr diagram. Shukolyukov and Lugmair (2006) reported that the correlation line yields a ^{53}Mn/^{55}Mn of 8.5 ± 1.5 × 10^{-6} and initial ε^{53}Cr = −0.21 ± 0.09 at the time of Mn/Cr fractionation. Göpel *et al.* (2015) obtained a $(^{53}Mn/^{55}Mn)_i$ = 6.24 × 10^{-6} and $\varepsilon^{53}Cr_i$ = −0.15 ± 0.10 from the bulk rock CC isochron. Based on this value and with respect to the age of the solar system, the authors determined solar system initial $(^{53}Mn/^{55}Mn)_i$ = 6.8 ± 0.66 × 10^{-6} and corresponding initial $\varepsilon^{53}Cr_i$ = −0.177 (see Fig. 8 in Gopel *et al*., 2015). It is important to note that ^{55}Mn/^{52}Cr *vs.* ^{53}Cr/^{52}Cr diagram for bulk rock CC is sensitive to the choice of samples that are included into the regression calculation (Gopel *et al*., 2015; Zhu *et al*., 2021). Trinquier *et al.* (2008b) constrained $(^{53}Mn/^{55}Mn)_i$ = 6.28 ± 0.66 × 10^{-6} using an isochron based on ^{54}Cr-poor fractions of CI Orgueil and reported it as the best estimate for the solar system initial ^{53}Mn abundance. However, Zhu *et al.* (2021) reported that the ^{53}Mn–^{53}Cr correlation could be a

mixing line since chondritic components, *e.g.*, CAIs, chondrules, matrix, metal, and carbonates have different origins and time of formation. To obtain the solar system initial $\varepsilon^{53}Cr_i$, Trinquier *et al.* (2008b) back-calculated $\varepsilon^{53}Cr_i$ for a wide range of chondritic reservoirs using present-day $^{53}Cr/^{52}Cr$ and Mn/Cr ratios to the time of CAI formation and reported the average of all $\varepsilon^{53}Cr_i$ as solar system initial $\varepsilon^{53}Cr_i = -0.23 \pm 0.09$. Nyquist *et al.* (2009) used a correlation regression between initial $(^{53}Mn/^{55}Mn)_i$ and initial $(^{26}Al/^{27}Al)_i$ for solar system materials that have been analysed by both Mn–Cr and Al–Mg chronometers to determine the value of initial $(^{53}Mn/^{55}Mn)_{SS} = (9.1 \pm 1.7) \times 10^{-6}$ corresponding to the assumed $(^{26}Al/^{27}Al)_{SS} = 5.1 \times 10^{-5}$. In the present study, the solar system initial $\varepsilon^{53}Cr_i = -0.30 \pm 0.05$ is proposed after calibrating the Mn–Cr model ages for the core formation in magmatic iron meteorite to the corresponding Hf–W core formation ages. The proposed value agrees with the previously reported solar system initial $\varepsilon^{53}Cr_i$ values. Additionally, it also agrees with solar system initial $\varepsilon^{53}Cr_i = -0.34$ when $(^{53}Mn/^{55}Mn)_i = 3.16 \pm 0.11 \times 10^{-6}$ and $\varepsilon^{53}Cr_i = -0.10 \pm 0.06$ (Zhu *et al.*, 2019) determined for bulk rock angrites are calibrated against the age of the solar system.

Supplementary Tables

Table S-1 $\varepsilon^{53}Cr$ and $\varepsilon^{54}Cr$ compositions of studied samples.

						$\varepsilon^{53}Cr$			$\varepsilon^{54}Cr$		
		$\varepsilon^{53}Cr$	s.e. int.[a]	$\varepsilon^{54}Cr$	s.e. int.[a]	mean	2 s.d. ext.[b]	2 s.e. ext.[b] (*n*)	mean	2 s.d. ext.[b]	2 s.e. ext.[b] (*n*)
IIAB											
Agoudal (Chr)	AG_36_1	−0.289	0.027	−0.895	0.055	−0.210	0.081	0.023 (12)	−0.784	0.206	0.060 (12)
	AG_36_1b	−0.161	0.024	−0.875	0.051						
	AG_36_1c	−0.197	0.027	−0.761	0.054						
	AG_36_1d	−0.235	0.027	−0.947	0.056						
	AG_36_1e	−0.251	0.028	−0.849	0.057						
	AG_36_3	−0.181	0.027	−0.752	0.058						
	AG_36_3b	−0.182	0.029	−0.789	0.059						
	AG_36_4	−0.187	0.031	−0.707	0.063						
	AG_36_5	−0.257	0.036	−0.693	0.074						
	AG_53_1	−0.234	0.032	−0.805	0.069						
	AG_53_2	−0.151	0.032	−0.792	0.062						
	AG_53_3	−0.193	0.029	−0.539	0.065						
Sikhote-Alin	SA_36_1	−0.159	0.028	−0.821	0.053	−0.228	0.087	0.025 (12)	−0.923	0.177	0.051 (12)
(Chr)	SA_36_2	−0.255	0.030	−1.014	0.062						
	SA_36_3	−0.249	0.026	−0.931	0.057						
	SA_36_4	−0.189	0.025	−1.036	0.059						
	SA_36_4b	−0.178	0.026	−0.972	0.049						
	SA_36_5	−0.237	0.025	−0.842	0.052						
	SA_36_5b	−0.253	0.024	−0.966	0.050						
	SA_53_1	−0.188	0.029	−0.846	0.060						
	SA_53_1b	−0.212	0.025	−0.813	0.052						
	SA_53_2	−0.231	0.029	−1.050	0.057						
	SA_53_3	−0.325	0.046	−0.803	0.078						
	SA_53_3b	−0.256	0.030	−0.978	0.062						

Table S-1 continued

						ε^{53}Cr			ε^{54}Cr		
		ε^{53}Cr	s.e. int.[a]	ε^{54}Cr	s.e. int.[a]	mean	2 s.d. ext.[b]	2 s.e. ext.[b] (*n*)	mean	2 s.d. ext.[b]	2 s.e. ext.[b] (*n*)
NWA 11420 (Daub)	Daub_37_2	−0.161	0.029	−0.808	0.063	−0.203	0.118	0.045 (7)	−0.768	0.147	0.055 (7)
	Daub_37_3	−0.183	0.031	−0.731	0.064						
	Daub_37_4	−0.131	0.026	−0.654	0.048						
	Daub_53_1	−0.161	0.029	−0.680	0.067						
	Daub_53_2	−0.222	0.024	−0.836	0.048						
	Daub_53_3	−0.320	0.032	−0.854	0.069						
	Daub_53_3b	−0.240	0.040	−0.810	0.077						
IIIIAB Cape York (Chr)	CY_41_1	−0.164	0.030	−0.672	0.062	−0.196	0.154	0.043 (13)	−0.780	0.223	0.062 (13)
	CY_41_2	−0.188	0.034	−0.888	0.067						
	CY_41_3	−0.109	0.034	−0.588	0.072						
	CY_41_3b	−0.042	0.029	−0.692	0.059						
	CY_41_2b	−0.099	0.032	−0.859	0.057						
	CY_41_1b	−0.182	0.030	−0.870	0.058						
	CY_40_1	−0.176	0.024	−0.635	0.046						
	CY_54_1	−0.240	0.045	−0.956	0.089						
	CY_54_2	−0.293	0.046	−0.766	0.082						
	CY_54_3	−0.236	0.030	−0.789	0.060						
	CY_54_1b	−0.227	0.039	−0.802	0.067						
	CY_54_2b	−0.272	0.033	−0.700	0.066						
	CY_54_3b	−0.318	0.048	−0.923	0.084						
Saint Aubin (Chr)	S'Aub_50_1	−0.273	0.033	−0.810	0.073	−0.268	0.091	0.029 (10)	−0.779	0.193	0.061 (10)
	S'Aub_50_3	−0.242	0.039	−0.710	0.083						
	S'Aub_50_2	−0.330	0.031	−0.634	0.063						
	S'Aub_54_1	−0.249	0.032	−0.903	0.068						
	S'Aub_54_1b	−0.256	0.031	−0.880	0.068						
	S'Aub_54_2	−0.326	0.033	−0.926	0.070						
	S'Aub_54_2b	−0.221	0.033	−0.763	0.069						
	S'Aub_54_3	−0.193	0.028	−0.669	0.061						
	S'Aub_54_3b	−0.333	0.028	−0.803	0.061						
	S'Aub_54_3c	−0.255	0.029	−0.696	0.061						
IVA Yanhuitlan (Daub)	Yan _55_1	−0.192	0.030	−0.351	0.057	−0.272	0.085	0.027 (10)	−0.468	0.193	0.061 (10)
	Yan _55_1b	−0.273	0.027	−0.587	0.056						
	Yan _55_2b	−0.254	0.032	−0.529	0.065						
	Yan _55_2b	−0.285	0.032	−0.397	0.067						
	Yan _55_2c	−0.335	0.027	−0.583	0.061						
	Yan _55_2d	−0.234	0.029	−0.502	0.063						
	Yan _55_3	−0.228	0.029	−0.269	0.058						
	Yan _55_3b	−0.290	0.029	−0.509	0.063						
	Yan _55_3c	−0.307	0.028	−0.449	0.063						
	Yan _55_3d	−0.319	0.030	−0.499	0.062						

Table S-1 continued

						ε^{53}Cr			ε^{54}Cr		
		ε^{53}Cr	s.e. int.[a]	ε^{54}Cr	s.e. int.[a]	mean	2 s.d. ext.[b]	2 s.e. ext.[b] (*n*)	mean	2 s.d. ext.[b]	2 s.e. ext.[b] (*n*)
Duchesne (Daub)	Duch_55_1c	−0.144	0.038	−0.680	0.087	−0.160	0.097	0.037 (7)	−0.487	0.413	0.156 (7)
	Duch_55_1d	−0.134	0.040	−0.753	0.086						
	Duch_55_1e	−0.203	0.044	−0.674	0.103						
	Duch_55_1f	−0.092	0.046	−0.286	0.099						
	Duch_55_1g	−0.171	0.041	−0.509	0.084						
	Duch_55_1x	−0.249	0.050	−0.311	0.104						
	Duch_55_1xx	−0.127	0.045	−0.198	0.104						
Standards											
IAG OKUM	OKUM_50_1	0.046	0.032	0.140	0.067	0.020	0.159	0.065 (7)	0.083	0.270	0.110 (7)
	OKUM_50_2	0.034	0.038	0.204	0.081						
	OKUM_50_3	0.013	0.029	0.057	0.063						
	OKUM_61_1	−0.054	0.029	0.114	0.064						
	OKUM_61_1b	−0.106	0.029	−0.231	0.064						
	OKUM_61_2	0.168	0.031	0.173	0.063						
	OKUM_61_2b	0.036	0.031	0.125	0.062						
Allende (CV)[c]	All1	0.045	0.031	0.967	0.061	0.072	0.132	0.066 (4)	0.881	0.241	0.120 (4)
	All1b	0.092	0.030	0.865	0.063						
	All2	−0.014	0.027	0.691	0.054						
	All2b	0.167	0.031	1.001	0.070						
Dergaon WR (H5)	D_W_63_1	0.057	0.031	−0.547	0.069	0.117	0.078	0.039 (4)	−0.380	0.244	0.122 (4)
	D_W_63_2b	0.138	0.035	−0.399	0.081						
	D_W_63_2	0.162	0.029	−0.203	0.060						
	D_W_63_1b	0.112	0.036	−0.371	0.080						
RF 529 WR (Acap)	Acap1	0.187	0.026	−0.677	0.058	0.122	0.089	0.045 (4)	−0.698	0.170	0.085 (4)
	Acap1b	0.077	0.026	−0.741	0.058						
	Acap2	0.138	0.029	−0.572	0.067						
	Acap2b	0.083	0.030	−0.801	0.064						

[a]s.e. int.: internal error (reported as 1 s.e.) for a single filament run consisted of 24 blocks with 20 cycles each (integration time = 8.389 s).

[b]s.d. ext. and s.e. ext.: external errors of the replicate measurements reported as 2 s.d. and 2 s.e., respectively. *n* = number of replicate measurements.

[c]Allende rock standard (Smithsonian standard powder, USNM 3529, Split 18 position 1).

Abbreviations: Daub, daubréelite; Chr, chromite; WR, whole rock; Acap, Acapulcoite.

Table S-2 Weighted mean $\varepsilon^{53}Cr$ and $\varepsilon^{182}W$ of combined IIAB, IIIAB and IVA groups and corresponding Mn–Cr and Hf–W model ages.

Sample	$\varepsilon^{53}Cr$	Mn–Cr Model age (Ma)	Iron meteorite group	$\varepsilon^{182}W$	Hf–W Model age (Ma)
Agoudal	−0.210 ± 0.023		IIAB	−3.40 ± 0.03	
Sikhote Alin	−0.228 ± 0.025		IIIAB	−3.35 ± 0.03	
NWA 11420	−0.203 ± 0.045		IVA	−3.32 ± 0.05	
Saint Aubin	−0.268 ± 0.029				
Cape York	−0.196 ± 0.043				
Yanhuitlan	−0.272 ± 0.027				
Duchesne	−0.160 ± 0.037				
Weighted mean	−0.227 ± 0.006	0.03 ± 0.06[a] 1.04 ± 0.08[b]	Weighted mean	−3.37 ± 0.01	1.04 ± 0.09

Errors associated with weighted means are given in 1 s.e.
Mn–Cr model ages are determined using $\varepsilon^{53}Cr_i = -0.23$[a] and $\varepsilon^{53}Cr_i = -0.30$[b] in Equation 1 (see main text). The procedure to determine Hf–W model ages is adopted from Kruijer *et al.* (2017) and determined using the following equation and parameters:

$$\Delta t = (-1/\lambda) \times \ln [(\varepsilon^{182}W_{sample} - \varepsilon^{182}W_{chondrites}/\varepsilon^{182}W_{SSI} - \varepsilon^{182}W_{chondrites})]$$

Δt represents the time elapsed since the start of the solar system, $\varepsilon^{182}W_{sample}$ represents the pre-exposure $\varepsilon^{182}W$ of any iron meteorite group (Kruijer *et al*., 2017), $\varepsilon^{182}W_{chondrites}$ is the composition of carbonaceous chondrites (−1.91 ± 0.08) (Kleine *et al*., 2004), $\varepsilon^{182}W_{SSI}$ is the solar system initial value of –3.49 ± 0.07 as obtained from CAIs (Kruijer *et al*., 2014), and λ is the decay constant of ^{182}Hf (0.078 ± 0.002 Myr^{-1}, 2σ; Vockenhuber *et al*., 2004). A better fit between Mn–Cr and Hf–W model ages is obtained when Mn–Cr model ages are determined using $\varepsilon^{53}Cr = -0.30$.

Table S-3 Summary of $(^{53}Mn/^{55}Mn)_i$ and $(\varepsilon^{53}Cr)_i$.

$(^{53}Mn/^{55}Mn)_i$	$(\varepsilon^{53}Cr)_i$	References	Method/Approach
$(8.5 \pm 1.5) \times 10^{-6}$	−0.21 ± 0.09	Shukolyukov and Lugmair (2006)	Bulk CC isochron
$(6.53 \pm 1.93) \times 10^{-6}$	−0.23 ± 0.11	Trinquier *et al.* (2008b)	Inner solar system
$(6.28 \pm 0.66) \times 10^{-6}$		Trinquier *et al.* (2008b)	Orgueil (CI1) leachates
$(9.1 \pm 1.7) \times 10^{-6}$		Nyquist *et al.* (2009)	Best Estimate from $(^{53}Mn/^{55}Mn)_i$ *vs.* $(^{26}Al/^{27}Al)_i$
6.8×10^{-6}	−0.177	Göpel *et al.* (2015)	Bulk CC isochron calibrated against the solar system age
	−0.30 ± 0.05	This study	Proposed from combined Mn–Cr and Hf–W chronometry of IIAB, IIIAB and IVA iron meteorite groups

Supplementary Figures

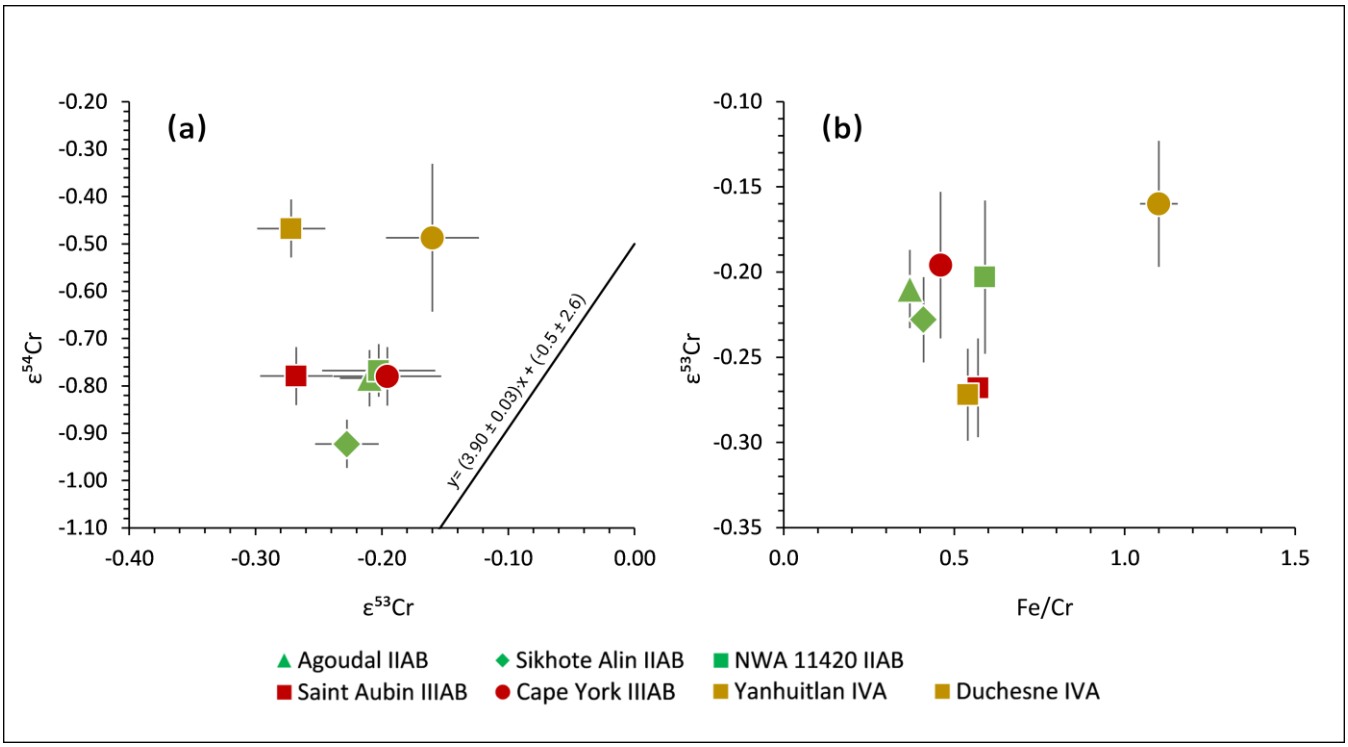

Figure S-1 **(a)** ε^{53}Cr *vs.* ε^{54}Cr and **(b)** Fe/Cr *vs.* ε^{53}Cr plots for the analysed iron meteorite samples. The black line in **(a)** shows a linear correlation between excesses in ε^{54}Cr and ε^{53}Cr [$y = (3.90 \pm 0.03)x + (-0.5 \pm 2.6)$ (95 % conf.)] determined by Liu *et al.* (2019) for iron meteorites analysed by Qin *et al.* (2010), Bonnand and Halliday (2018) and Liu *et al.* (2019). The error on the correlation line is not shown for the sake of clarity. The ε^{54}Cr and ε^{53}Cr values show no correlation for the analysed chromite/daubréelite fractions, corroborating the negligible spallogenic contribution in these components.

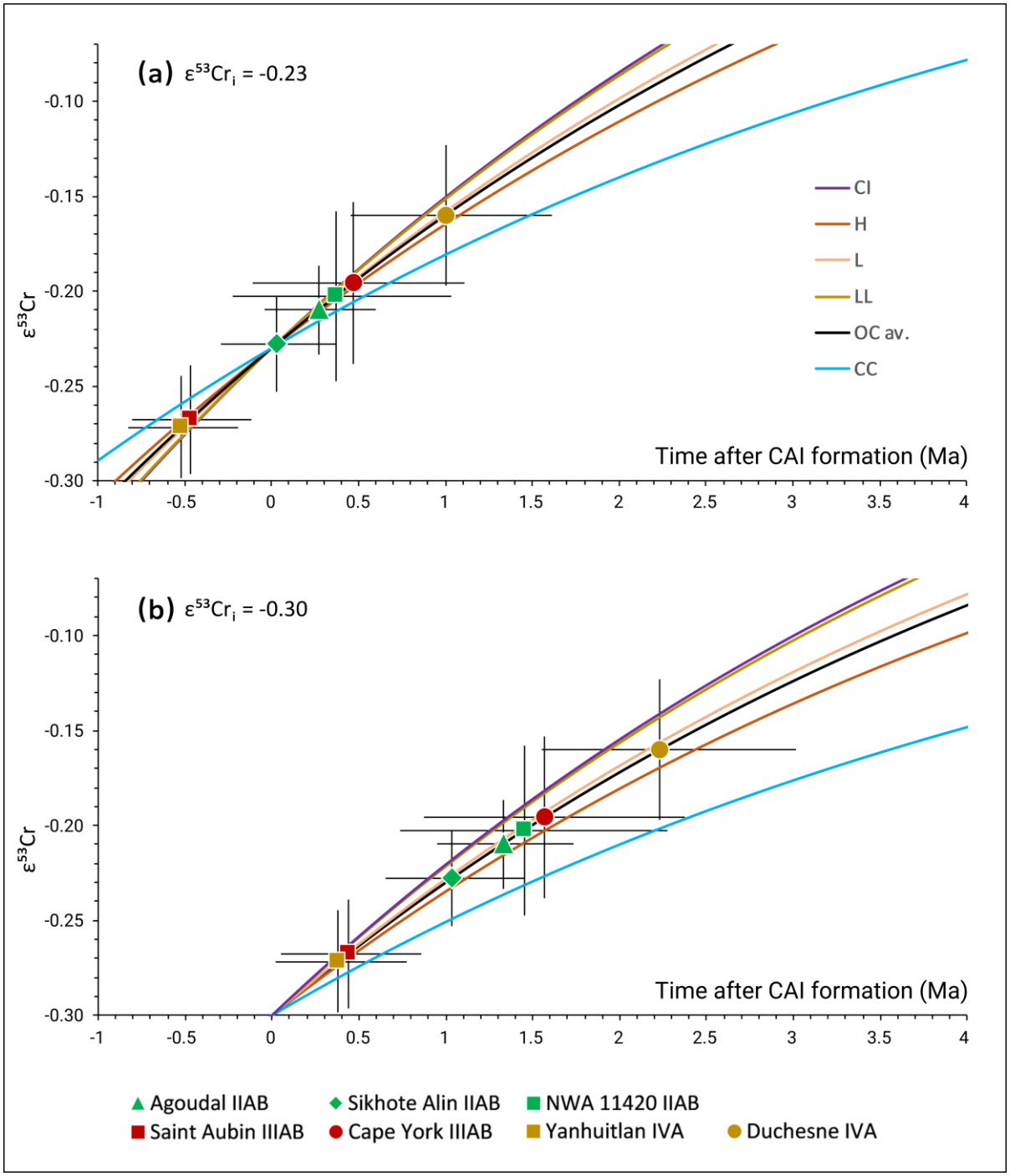

Figure S-2 Mn–Cr model ages plotted on an $\varepsilon^{53}Cr$ evolution curve using Equation 1 and solar system initial values of **(a)** $\varepsilon^{53}Cr_i = -0.23$ from Trinquier *et al.* (2008b) and **(b)** $\varepsilon^{53}Cr_i = -0.30$ as proposed in the present study (see main text for the model age calculation). Different evolutionary paths represent different Mn/Cr ratios of the parent bodies. The trajectories are derived using Equation 1 with the following Mn/Cr ratios: CI chondrites (0.84), H chondrites (0.69), L chondrites (0.76), LL chondrites (0.83), combined OCs (0.74) and combined CC chondrites (0.52) (Zhu *et al.*, 2021). Error bars represent 2 s.e. uncertainties. Model ages for IIAB, IIIAB and IVA groups are unaffected by the growth trajectory chosen, given current analytical resolution. Assuming a Mn/Cr similar to carbonaceous chondrites would change the model ages by a maximum of 1 Ma for the youngest sample. However, since all samples belong to the non-carbonaceous group, the average composition of OCs is most appropriate.

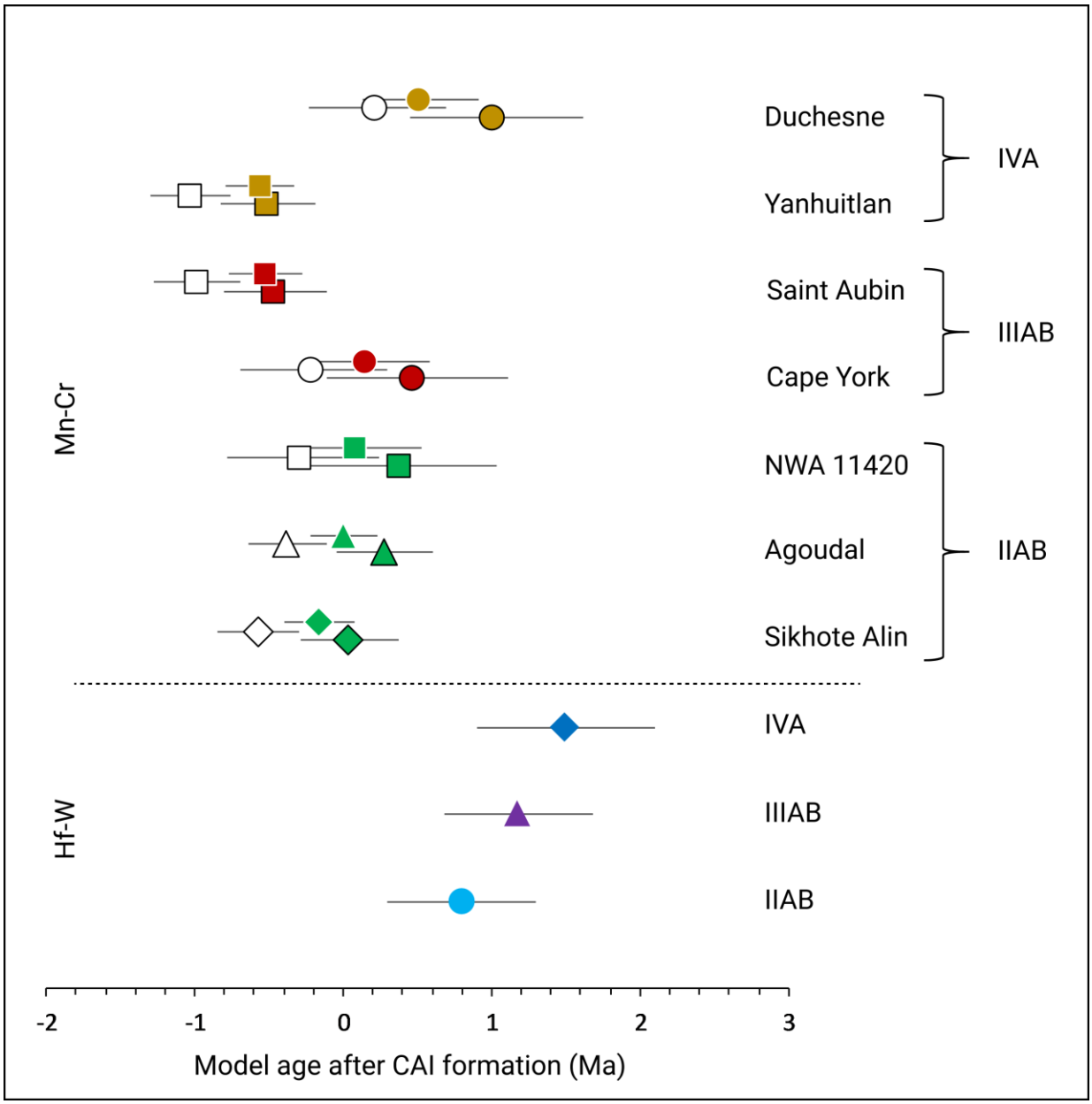

Figure S-3 Mn–Cr (present study) and Hf–W (Kruijer *et al.*, 2017) core formation ages. Mn–Cr model ages for each sample are determined using solar system initial $\varepsilon^{53}Cr_i$ and canonical $(^{53}Mn/^{55}Mn)_{ss}$ values taken from Trinquier *et al.* (2008b; coloured symbols, black borders), Göpel *et al.* (2015; coloured, no borders), and Shukolyukov and Lugmair (2006; white symbols).

Supplementary Information References

Birck, J.L., Allègre, C.J. (1985) Isotopes produced by galactic cosmic rays in iron meteorites. In: Gautier, D. (Ed.) *Isotopic ratios in the solar system*. Centre National d'Etudes Spatiales, Editions Cépaduès, Toulouse, 21–25.

Bonnand, P., Halliday, A.N. (2018) Oxidized conditions in iron meteorite parent bodies. *Nature Geoscience* 11, 401–404.

Göpel, C., Birck, J.L., Galy, A., Barrat, J.A., Zanda, B. (2015) Mn–Cr systematics in primitive meteorites: Insights from mineral separation and partial dissolution. *Geochimica et Cosmochimica Acta* 156, 1–24.

Kleine, T., Mezger, K., Palme, H., Münker, C. (2004) The W isotope evolution of the bulk silicate Earth: Constraints on the timing and mechanisms of core formation and accretion. *Earth and Planetary Science Letters* 228, 109–123.

Kruijer, T.S., Kleine, T., Fischer-Gödde, M., Burkhardt, C., Wieler, R. (2014) Nucleosynthetic W isotope anomalies and the Hf–W chronometry of Ca-Al-rich inclusions. *Earth and Planetary Science Letters* 403, 317–327.

Kruijer, T.S., Burkhardt, C., Budde, G., Kleine, T. (2017) Age of Jupiter inferred from the distinct genetics and formation times of meteorites. *Proceedings of the National Academy of Sciences* 114, 6712–6716.

Liu, J., Qin, L., Xia, J., Carlson, R.W., Leya, I., Dauphas, N., He, Y. (2019) Cosmogenic effects on chromium isotopes in meteorites. *Geochimica et Cosmochimica Acta* 251, 73–86.

Moynier, F., Yin, Q.Z., Jacobsen, B. (2007) Dating the first stage of planet formation. *The Astrophysical Journal Letters* 671, 181.

Nyquist, L.E., Kleine, T., Shih, C.Y., Reese, Y.D. (2009) The distribution of short-lived radioisotopes in the early solar system and the chronology of asteroid accretion, differentiation, and secondary mineralization. *Geochimica et Cosmochimica Acta* 73, 5115–5136.

O'Hara, M.J., Kellogg, C.M., Parker, C.M., Morrison, S.S., Corbey, J.F., Grate, J.W. (2017) Decomposition of diverse solid inorganic matrices with molten ammonium bifluoride salt for constituent elemental analysis. *Chemical Geology* 466, 341–351.

Qin, L., Alexander, C.M.O'D., Carlson, R.W., Horan, M.F., Yokoyama, T. (2010) Contributors to chromium isotope variation of meteorites. *Geochimica et Cosmochimica Acta* 74, 1122–1145.

Schoenberg, R., von Blanckenburg, F. (2005) An assessment of the accuracy of stable Fe isotope ratio measurements on samples with organic and inorganic matrices by high-resolution multicollector ICP-MS. *International Journal of Mass Spectrometry* 242, 257–272.

Schoenberg, R., Merdian, A., Holmden, C., Kleinhanns, I.C., Haßler, K., Wille, M., Reitter, E. (2016) The stable Cr isotopic compositions of chondrites and silicate planetary reservoirs. *Geochimica et Cosmochimica Acta* 183, 14–30.

Shields, W.R., Murphy, T.J., Catanzaro, E.J., Garner, E.L. (1966) Absolute isotopic abundance ratios and the atomic weight of a reference sample of chromium. *Journal of Research of the National Bureau of Standards Section A: Physics and Chemistry* 70A, 193.

Shukolyukov, A., Lugmair, G.W. (2006) Manganese–chromium isotope systematics of carbonaceous chondrites. *Earth and Planetary Science Letters* 250, 200–213.

Trinquier, A., Birck, J.L., Allègre, C.J. (2007) Widespread ^{54}Cr heterogeneity in the inner solar system. *The Astrophysical Journal* 655, 1179–1185.

Trinquier, A., Birck, J.L., Allègre, C.J. (2008a) High-precision analysis of chromium isotopes in terrestrial and meteorite samples by thermal ionization mass spectrometry. *Journal of Analytical Atomic Spectrometry* 23, 1565–1574.

Trinquier, A., Birck, J.L., Allègre, C.J., Göpel, C., Ulfbeck, D. (2008b) ^{53}Mn–^{53}Cr systematics of the early Solar System revisited. *Geochimica et Cosmochimica Acta* 72, 5146–5163.

Vockenhuber, C., Oberli, F., Bichler, M., Ahmad, I., Quitté, G., Meier, M., Halliday, A.N., Lee, D.C., Kutschera, W., Steier, P., Gehrke, R.J. (2004) New half-life measurement of ^{182}Hf: Improved chronometer for the early solar system. *Physical Review Letters* 93, 172501.

Yamakawa, A., Yamashita, K., Makishima, A., Nakamura, E. (2009) Chemical separation and mass spectrometry of Cr, Fe, Ni, Zn, and Cu in terrestrial and extra-terrestrial materials using thermal ionization mass spectrometry. *Analytical Chemistry* 81, 9787–9794.

Zhu, K., Moynier, F., Wielandt, D., Larsen, K.K., Barrat, J.A., Bizzarro, M., (2019) Timing and origin of the angrite parent body inferred from Cr isotopes. *The Astrophysical Journal Letters* 877, L13.

Zhu, K., Moynier, F., Schiller, M., Alexander, C.M.O'D., Davidson, J., Schrader, D.L., van Kooten, E., Bizzarro, M. (2021) Chromium isotopic insights into the origin of chondrite parent bodies and the early terrestrial volatile depletion. *Geochimica et Cosmochimica Acta* 301, 158–186.